

Estimation of baseline phase and iron concentrations in the macaque brain

Jason Langley¹, Longchuan Li¹, Xiaodong Zhang², and Xiaoping Hu¹

¹Department of Biomedical Engineering, Emory University and Georgia Institute of Technology, Atlanta, Georgia, United States, ²Division of Neuroscience, Yerkes National Primate Research Center, Atlanta, Georgia, United States

INTRODUCTION

There has been renewed focus on quantification of iron in the brain particularly since iron is thought to play a key role in aging, Parkinson's disease, and Alzheimer's disease. A procedure that is useful in visualizing iron containing regions is susceptibility weighted imaging (SWI). SWI provides a contrast that is loosely based on the susceptibility of the underlying tissues and uses high pass filtered phase maps to generate the contrast. Recent work (1-4) has shown high pass filtered phase maps, acquired using a susceptibility weighted gradient echo sequence, can be used to estimate iron content within the brain. Other methods to estimate iron content within the brain include mapping T_2 , T_2^* , or T_2' (5) and a study (6) has shown that there is a correlation between the relaxation rate method and the phase-based method in certain structures within the human brain, particularly within the putamen. In this abstract, high pass filtered phase maps are used to estimate the iron content in four different structures within the macaque brain to gain baseline estimates on the iron content in a young and healthy macaque brain.

MATERIALS AND METHODS

Phase maps are sensitive to inhomogeneities in the magnetic field and the following relationship between the phase, denoted ϕ , and the magnetic field inhomogeneities, denoted ΔB , describes the relationship between phase maps and the field inhomogeneities

$$\phi = -\gamma\Delta BTE + \phi_0 \quad [1]$$

where γ denotes the gyromagnetic ratio of Hydrogen, ϕ_0 denotes the phase offset, and TE denotes the echo time. The dependence of the magnetic field inhomogeneities on iron concentration can be expressed using the following relationship:

$$\Delta B = c\Delta\chi VB_0 \quad [2]$$

where V is the volume of the voxel, c is the concentration of iron in the voxel, and $\Delta\chi$ is the change in molar susceptibility between tissues where iron is present (1).

To estimate the iron within the brain, the phase map from each subject was high pass filtered. The process of high pass filtering was as follows: first a low pass phase map was constructed by convolving a Hamming window with the wrapped phase map; next the complex difference was taken of the low pass phase map and the wrapped phase map. Next, SWI images were used to identify the putamen, cuneus, caudate nucleus, and globus pallidus for each subject. Regions of interest were drawn within each structure and the mean of the high pass phase within each region of interest was calculated.

Six healthy female macaques were scanned in this study and average age of the cohort was 8.2 years with a standard deviation of 1.3 years old. A three-dimensional susceptibility weighted gradient echo pulse sequence with the following parameters was used to acquire the data sets: echo time (TE) / repetition time (TR) = 20 / 28 ms; field of view = 97 × 114 mm; matrix size = 448 × 364 × 56; slice thickness = 1 mm; flip angle = 15 degrees; averages = 2. All data sets were acquired on a Siemens 3 T Trio (Siemens Medical Solutions, Malvern, Pennsylvania) and all data analysis was performed in MATLAB (The MathWorks, Natick, Massachusetts).

RESULTS AND DISCUSSION

The mean of different regions in high passed phase map is shown in Table 1. Hopp, *et al* calibrated the relationship between the phase difference and iron content using x-ray fluorescence and found the following relationship between phase difference and iron content in human brains (1):

$$c_{Fe} = 850\Delta\phi(1.5/B_0)(20/TE) + 110 \quad [3]$$

where B_0 denotes the strength of the magnetic field and c_{Fe} is the iron content in units of ($\mu\text{g} / \text{g}$ tissue). This relationship gives a rough estimate of the iron content in the macaque brain and the iron estimates for different regions are shown in Table 1. The error bars in Table 1 show the standard error across all six subjects. One possible explanation for the large error bars in Table 1 is the low SNR of the data sets. The mean SNR across subjects was 12.4 with a standard deviation of 2.34.

It should be noted that, although the phase of a voxel is dependent on the iron content within the voxel, other factors might influence the phase within the voxel. These factors include the geometry of the regions analyzed and their orientation within the main magnetic field, magnetic field inhomogeneities generated by tissue/tissue, air/tissue, or fluid/tissue interfaces, and field inhomogeneities. Additional irregularities can be added since this method only detects paramagnetic iron.

	Putamen	Cuneus	Caudate Nucleus	Globus Pallidus
Mean Phase for Macaque (Radians)	0.0221±0.016	0.0308±0.0057	0.0041±0.0032	-0.0541±0.012
Iron Content for Macaque ($\mu\text{g} / \text{g}$ tissue)	203.9±178.0	240.9±112.4	111.7±111.36	
Mean Phase for Human (Radians)	0.0421±0.001	Not Measured	0.00617±0.001	-0.087±0.034
Iron Content for Human ($\mu\text{g} / \text{g}$ tissue)	127.9±110.4	Not Measured	112.6±110.4	

Table 1. The results from the iron quantification process applied to the six data sets considered in this abstract. As a comparison, human measurements from (4) are shown for the putamen and the caudate nucleus. Human measurements from (1) are shown for the globus pallidus. The iron content (shown in row two) for the putamen, cuneus, and caudate nucleus was estimated using equation [3].

In summary, the phase values we found in the putamen and caudate nucleus accord well with previously published results shown in humans (3,4). Furthermore, we see that the putamen and globus pallidus, and cuneus, contains more iron than the caudate nucleus.

REFERENCES

- (1) Haacke, *et al.* JMRI 26:256 2007; (3) Pfefferbaum, *et al.* Neuroimage 47:493 2009; (5) Ordidge, *et al.* MRM 32:335 1994
 (2) Hopp, *et al.* JMRI 31:1346 2010; (4) Zhang, *et al.* Neurosci Bull 25:353 2009; (6) Haacke, *et al.* JMRI 32:561 2010

Acknowledgement: This work was kindly supported by NIH 5P01 AG026423-03

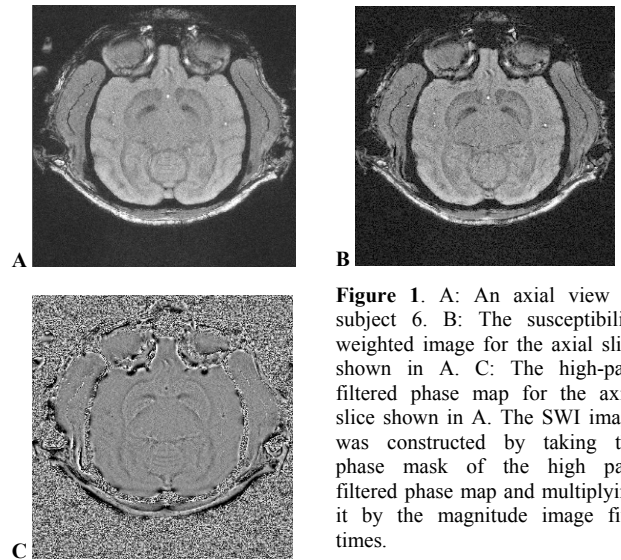


Figure 1. A: An axial view of subject 6. B: The susceptibility weighted image for the axial slice shown in A. C: The high-pass filtered phase map for the axial slice shown in A. The SWI image was constructed by taking the phase mask of the high pass filtered phase map and multiplying it by the magnitude image five times.